Comprehensive plaque assessment by coronary CT angiography

Pál Maurovich-Horvat, Maros Ferencik, Szilard Voros, Béla Merkely and Udo Hoffmann

Abstract | Most acute coronary syndromes are caused by sudden luminal thrombosis due to atherosclerotic plaque rupture or erosion. Preventing such an event seems to be the only effective strategy to reduce mortality and morbidity of coronary heart disease. Coronary lesions prone to rupture have a distinct morphology compared with stable plaques, and provide a unique opportunity for noninvasive imaging to identify vulnerable plaques before they lead to clinical events. The submillimeter spatial resolution and excellent image quality of modern computed tomography (CT) scanners allow coronary atherosclerotic lesions to be detected, characterized, and quantified. Large plaque volume, low CT attenuation, napkin-ring sign, positive remodelling, and spotty calcification are all associated with a high risk of acute cardiovascular events in patients. Computation fluid dynamics allow the calculation of lesion-specific endothelial shear stress and fractional flow reserve, which add functional information to plaque assessment using CT. The combination of morphologic and functional characteristics of coronary plaques might enable noninvasive detection of vulnerable plaques in the future.

Maurovich-Horvat, P. *et al. Nat. Rev. Cardiol.* advance online publication 22 April 2014; doi:10.1038/nrcardio.2014.60

Introduction

Cardiovascular diseases are the number one cause of death globally. The number of people who die from cardiovascular diseases, mainly from coronary heart disease and stroke, will increase to reach 23.3 million by 2030 from an estimated 17.3 million deaths in 2008. Cardiovascular diseases are projected to remain the single leading cause of death by 2030 globally.[1,2] In 2014, an estimated 1.1 million people in the USA will have a major adverse coronary event, which will lead to death in ~34% of those individuals, despite many effective treatment strategies existing to lower cardiovascular risk.[3] Furthermore, by 2030, the prevalence of coronary artery disease (CAD) in the USA is predicted to increase by 16.6%—from 8.0% (based on 2010 estimates) to nearly 9.5%.[3,4] Acute myocardial infarction and sudden cardiac death remain the first manifestations of coronary atherosclerosis in the majority of the population (in 50% of men and 64% of women), which accounts for these unfavourable statistics.[5,6] Most individuals do not, therefore, experience any symptoms or warning signs before the coronary event (acute coronary syndromes [ACS] or sudden cardiac death) occurs.

Prevention of acute coronary events seems to be the only effective strategy to reduce the burden of cardiovascular disease and improve mortality and morbidity rates.[7,8] Considerable efforts are ongoing to predict where acute coronary events will happen on an individual plaque level. The identification of patients at high risk of developing acute coronary events remains a major challenge in cardiovascular imaging.[4,8,9] Current diagnostic strategies focus predominantly on the detection of myocardial ischaemia and haemodynamic luminal narrowing, but not the detection and characterization of coronary atherosclerotic plaques.[6] This strategy is based on the evaluation of symptomatic patients and ignores the larger problem of a major adverse coronary events occurring as the first (and only) manifestation of CAD.

In *post-mortem* studies, most acute coronary events are found to be caused by sudden luminal thrombosis due to plaque rupture.[10–12] The morphology of atherosclerotic plaques that are prone to rupture is distinct from stable lesions (Figure 1), which provides a unique opportunity for noninvasive imaging to identify high-risk plaques before they lead to adverse clinical events.[13,14] Moreover, the assessment of coronary plaque composition and size are potentially more important than traditional detection of luminal stenosis for predicting devastating acute coronary events.[11,15,16] Coronary computed tomography angiography (CCTA) permits the noninvasive evaluation of the coronary atherosclerotic plaque, not just the coronary lumen.[17] CCTA provides information regarding the coronary tree and atherosclerotic plaques beyond simple luminal narrowing and plaque type defined by calcium content.[17,18] These novel applications will improve image-guided prevention, medical therapy, and coronary interventions. The ability to interpret CCTA images beyond the coronary lumen and stenosis is of utmost importance as we develop personalized medical care to enable therapeutic interventions stratified on the basis of plaque characteristics.

In this Review, we describe the morphological and functional features of vulnerable plaques, as potential

MTA-SE Lendület Cardiovascular Imaging Research Group, Heart and Vascular Centre, Semmelweis University, 68 Varosmajor ut, 1025 Budapest, Hungary (**P.M-H.**, **B.M.**). Cardiac MR PET CT Program, Division of Cardiology and Department of Radiology, Massachusetts General Hospital, Harvard Medical School, 165 Cambridge Street, Suite 400, Boston, MA 02114. USA (**M.F.**, **U.H.**). Stony Brook University, 101 Nicolls Road, Stony Brook, NY 11794 USA (**S.V.**).

Correspondence to: U.H. uhoffmann@mgh.harvard.edu

Competing interests
The authors declare no competing interests

Key points

- Most acute coronary events result from sudden luminal thrombosis due to rupture of an atherosclerotic plaque
- Modern computed tomography (CT) scanners enable robust coronary plaque characterization and quantification
- Large plaque volume, low CT attenuation, napkin-ring sign, positive remodelling, and spotty calcification are all associated with plaques vulnerable to rupture
- Computational fluid dynamic simulation enables plaque-specific endothelial shear stress and fractional flow reserve assessment, and thus permits functional characterization of plaques
- Coupling individual plaque morphology with plaque-specific functional data will enable new noninvasive detection of vulnerable plaques with CT

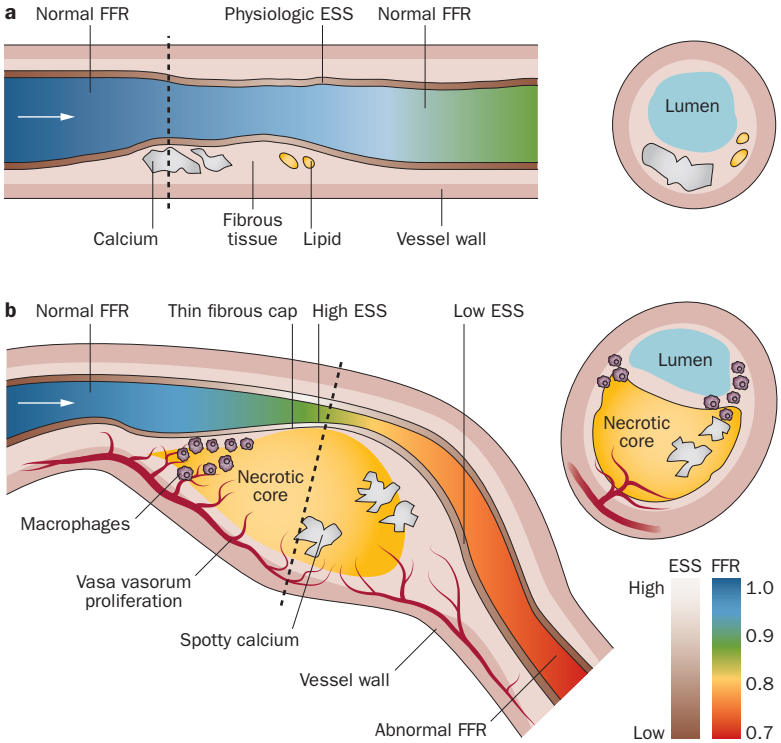

Figure 1 | The morphology and functional characteristics of stable and vulnerable plaques. **a** | Stable fibrocalcific lesion with calcification and small lipid pools. The plaque leads to mild narrowing of the lumen; however, there is no ischaemia after the lesion (FFR >0.8; green). ESS near the plaque is in the normal physiological range indicating undisturbed flow. **b** | Rupture prone vulnerable plaque with a large lipid-rich necrotic core, thin fibrous cap, neovascularization, spotty calcium and presence of inflammatory cells. Despite the positively remodelled vessel wall at the site of the plaque, the lesion causes severe luminal narrowing and ischaemia (FFR <0.8; red). The downstream plaque region with low and oscillatory ESS promotes plaque growth, whereas the upstream low ESS at the shoulder regions is more inflamed (indicated by presence of macrophages), which might lead to plaque destabilization. High ESS at the most stenotic part can trigger plaque rupture. Abbreviations: ESS, endothelial shear stress; FFR, fractional flow reserve. Part b modified with permission from Nature Publishing Group © Slager, C. J. *et al.* The role of shear stress in the destabilization of vulnerable plaques and related therapeutic implications. *Nat. Clin. Pract. Cardiovasc. Med.* **2**, 456–464 (2005).[89]

targets of conventional CCTA imaging. We also highlight novel image post-processing techniques and integrated computational fluid dynamics simulations to characterize coronary plaques and stenoses. Finally, we discuss future imaging techniques for atherosclerotic plaque detection and potential strategies to identify patients at highest risk of developing ACS.

Plaque morphology

Histological investigations have revealed three distinct features of plaques associated with acute coronary events: rupture; erosion; and calcified nodule.[19] Two-thirds of luminal thrombi in acute events result from ruptured atherosclerotic lesions characterized by a necrotic core covered by a thin layer of fibrous cap (Figure 1b).[19] Plaques vulnerable to rupture might have the same morphological characteristics as ruptured plaques, but with an intact thin fibrous cap.[12] These lesions—termed thin-cap fibroatheroma (TCFA), with a cap thickness of <65 μm—are considered to be the precursor lesions of plaque rupture.[19] The limited spatial resolution of current CT scanners (≈400 μm) precludes the morphometric analysis of fibrous cap by CCTA.[20] Histopathological investigations suggest that plaques prone to rupture are enlarged in all three spatial dimensions.[19,21] In TCFAs the necrotic core length is ~2–17 mm (mean 8 mm) and the area of the necrotic core in 80% of cases is >1.0 mm^2.[4,19] These dimensions are over the plaque detection threshold (>1 mm plaque thickness) for CCTA.[22] Moreover, the majority of TCFAs occur in the proximal portions of the main coronary arteries, where vessel diameter is largest, and CCTA has the highest image quality and accuracy for the plaque detection.[19,23] In modern CT scanners, the detection and quantification of some features of high-risk lesions might, therefore, be feasible (Supplementary Table 1 online).

Coronary plaque burden

Large plaque volume was associated with the diagnosis of ACS in cross-sectional studies, and quantification of noncalcified plaques (NCP) can improve risk stratification and improve the prognostic value of CCTA to predict future cardiovascular events. The multicentre Providing Regional Observations to Study Predictors of Events in the Coronary Tree (PROSPECT) trial[24] is the first and largest natural-history study of coronary plaques using invasive angiography and intravascular ultrasound (IVUS) to identify plaques vulnerable to rupture on a per-lesion basis.[24] The prospective study included 697 patients with ACS in whom 3-vessel grey-scale IVUS and IVUS with radiofrequency backscatter analysis (known as virtual histology IVUS [VH-IVUS]) were performed to characterize nonculprit (that is unruptured) lesions. After a median of 3.4 years follow-up, the strongest predictor of future events was the IVUS-derived plaque burden of ≥70% (HR 5.03; 95% CI 2.51–10.11; P <0.001).[24]

CT data sets can provide submillimeter isotropic spatial resolution, and the possibility of CT attenuation-based tissue characterization enable the quantification of total coronary plaque burden and individual plaque components, which is similar to the results obtained with IVUS.[25–29] Automated software tools are now available for plaque quantification and characterization (Figure 2). Automated quantification of plaques is desirable to improve the reproducibility, accuracy and efficiency of CCTA plaque analysis. The reproducibility of automated 3D quantification software for plaque burden was

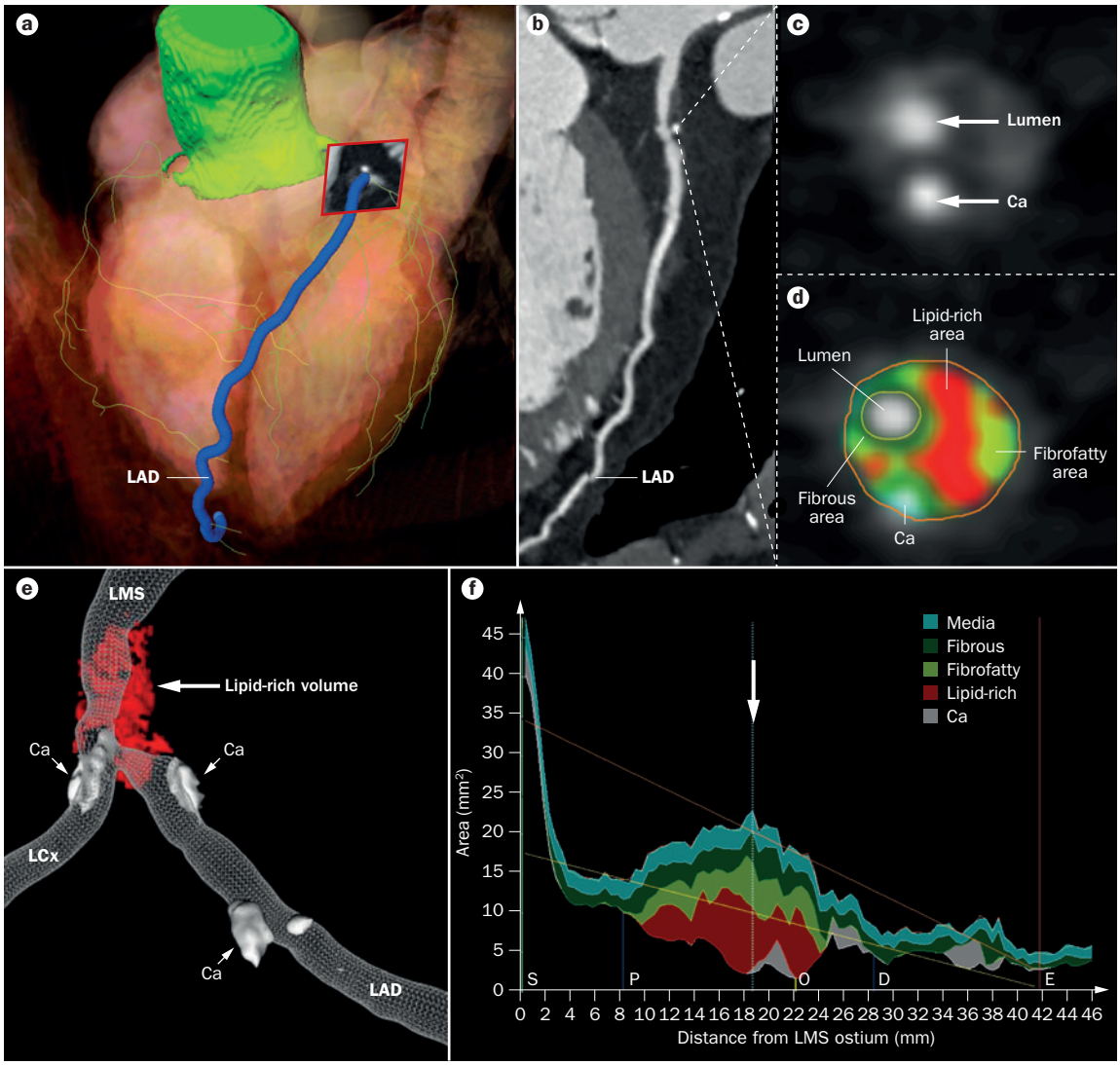

Figure 2 | Example of plaque characterization and quantification using a dedicated automated software tool and CCTA data set. **a** | Segmented whole coronary tree. The LAD is indicated in blue. The coronary centrelines and the aorta are indicated in green. Red box indicates plaque of interest. **b** | Curved multiplanar reconstruction of the LAD. Dotted lines indicate a partially calcified, positively remodelled plaque in the LMS bifurcation. **c** | The LMS plaque cross-section from panel b. **d** | The LMS plaque cross-section with colour overlay derived with adaptive threshold setting. The lipid rich (low CT attenuation) plaque components are shown in red. Fibro-fatty tissue is shown in light-green. Fibrous tissue is shown in dark-green. Calcium is shown in white. **e** | Volumetric assessment of the lipid rich plaque core is shown in red, and the core's spatial relation to the lumen (grey mesh) and calcium (white). **f** | The graph illustrates the areas of different plaque components. The colour scheme is identical to panel d. Abbreviations: Ca, calcium; CCTA, coronary computed tomography angiography; LAD, left anterior descending artery; LCx, left circumflex coronary artery; LMS, left main stem.

demonstrated to be excellent, with an intraclass correlation (ICC) value of 0.88 (95% CI 0.74–0.95); excellent agreement was defined as an ICC coefficient of >0.8.[30] The accuracy of automated coronary plaque quantification by CCTA was successfully validated against greyscale IVUS and VH-IVUS.[30–32] However, automated plaque quantification software tools have poor interplatform reproducibility; the same software should, therefore, be used for serial or comparative assessments.[33]

The culprit lesion (that is ruptured) and vulnerable plaques evaluated by histology or invasive imaging techniques tend to be large in size, leading to the hypothesis that CCTA quantification might incrementally improve risk stratification of patients over conventional CCTA reading.[13] A cross-sectional clinical investigation demonstrated that the culprit plaques in patients with ACS have larger volume than stable lesions in patients with stable angina pectoris (SAP; 193 mm^3 versus 104 mm^3; $P=0.001$).[34] In patients with unstable angina, quantitative CCTA revealed that plaques with morphological features of plaque disruption (such as intraplaque contrast dye penetration) had a larger volume compared with plaques that had no signs of disruption (313 ± 356mm^3 versus 118 ± 93 mm^3; $P<0.0001$). These lesions also contained more low CT attenuation components characteristic to lipid-rich plaques (99 ± 161 mm^3 versus 19 ± 18 mm^3;

$P<0.0001$) than undisrupted plaques.[35] In patients with acute chest pain and obstructive coronary lesions, the total volume of plaques leading to stenosis was not significantly different between those individuals with and those without ACS (212 mm^3 versus 171 mm^3; $P=0.24$). Interestingly, the volume of NCP with low CT attenuation density, (<90 Hounsfield units [HU], a measure of CT attenuation) was significantly larger in patients with ACS compared with patients who did not have ACS (91 mm^3 versus 49 mm^3; $P=0.03$).[16]

Longitudinal clinical investigations indicate a strong prognostic value of CCTA derived plaque volume for future coronary events. In a retrospective study of 1,059 patients with stable chest pain, the coronary plaque volume was larger in those patients who developed ACS compared with patients who did not during a follow-up period of 27 ± 10 months (134.9 ± 14.1 mm^3 versus 57.8 ± 5.7 mm^3; $P<0.001$).[36] The authors of a study published in 2013 elegantly demonstrated that semiautomatic plaque quantification—whereby plaques are manually identified before automatic segmentation, characterization, and quantification, with optional manual corrections—provided additional prognostic value for ACS over both clinical risk factors and traditional CT reading (including calcium score, segment stenosis score, lesion severity, and number of segments with NCP).[37] The patients who developed ACS had a higher total plaque volume (median 94 mm^3 versus 29 mm^3; $P<0.001$) and total NCP volume (28 mm^3 versus 4 mm^3; $P<0.001$) at baseline compared with those individuals who did not develop ACS.[37] The volume of nonobstructive NCP measured by CCTA was a strong predictor of future coronary events in a prospective study of 312 patients with non-ST-segment elevation myocardial infarction who underwent CCTA before invasive coronary angiography.[38] In total, 23 patients had a coronary event after a median follow-up of 16 months and the total volume of nonobstructive NCP was independently associated with the events with an HR of 1.18 per 100 mm^3 plaque volume increase. Interestingly, neither Agatston score (a measure of calcium content in a CT scan), nor calcified plaque volume were associated with an increased risk of coronary event.[38] A subset of patients ($n=32$) underwent CCTA in the PROSPECT study.[24,39] The authors of this exploratory substudy observed a higher total atheroma volume at baseline in patients with subsequent cardiac events during the mean 39 months follow-up (970 mm^3 versus 811 mm^3; $P<0.01$).[39]

However, despite these promising results, further software improvements are warranted to maximize accuracy, reproducibility, and time-efficiency before automated plaque burden quantification is implemented in the clinic.[40] Moreover, industry standards should be developed to enable reproducible plaque assessments with CCTA regardless of the software tool used.[33]

Low CT attenuation plaques

Lesions leading to ACS often have a large necrotic lipid-rich core; therefore, the CT differentiation between plaques containing lipid-rich material and plaques with predominantly fibrous components is desirable for prediction of ACS.[13] Traditionally, CCTA classifies plaques according to the presence or absence of calcified components, thereby differentiating between calcified, partially-calcified (mixed), and NCPs. The differentiation between calcified plaque components and NCPs was feasible even with early multidetector CT technology (such as 4-slice CTs used in the late 1990s).[41,42] However, the classification of NCPs into lipid-rich and fibrous lesions on the basis of CT attenuation values (measured by HU) remains challenging.

Some investigators have correlated CCTA plaque assessment with the clinical reference standard IVUS, and report low CT attenuation on average for lipid-rich plaques.[43] NCPs with high CT attenuation correlated with fibrous tissue and those with low densities correlated with necrotic core and fibrofatty tissue as assessed by VH-IVUS.[31] In histogram analysis of the intraplaque pixel CT numbers, lipid-rich plaques have a higher percentage of pixels with low HU values compared with plaques of predominantly fibrous components.[44] This observation was validated in an *ex vivo* study that showed that the relative area (area >25%) of intraplaque pixels with <60 HU could accurately detect lipid-rich atherosclerotic lesions (sensitivity, 73%; specificity, 71%).[45] Moreover, low CT numbers were measured in TCFAs identified by optical coherence tomography (OCT; the standard clinical reference for fibrous cap thickness measurements and necrotic lipid-rich core detection) compared with stable lesions (35–45 HU versus 62–79 HU; $P<0.001$).[46,47] However, the variability of CT values within plaque types is wide. Despite the differences in mean densities between fibrous plaques and lipid-rich plaques, almost all investigators have reported a substantial overlap of densities, which prevented the reliable subclassification of NCPs.[31,43] Furthermore, CT measurements of coronary plaques are influenced by several factors, such as the concentration of adjacent intraluminal iodinated contrast agent, plaque size, image noise, tube voltage, slice thickness, and the reconstruction filter.[48–51] The reliable differentiation between lipid-rich and fibrous lesions made solely on the basis of CT attenuation is, therefore, not yet feasible.[17] New automated plaque quantification software tools, with scan-specific adaptive attenuation threshold settings, can potentially overcome some of these limitations and might improve CT number-based plaque component quantification (Figure 2).[30,52]

Despite the challenges associated with CT number-based plaque characterization, low CT attenuation seems to be a consistent feature of lipid-rich plaques. Low-density plaques, defined by <30 HU average attenuation, were more often seen in patients with ACS than in those individuals with SAP (79% versus 9%; $P<0.0001$).[53] The same investigators compared the characteristics of ruptured fibrous cap culprit lesions in patients with ACS with the intact fibrous cap plaques of patients with SAP. Again, the low plaque attenuation was defined as <30 HU, and 88% of ruptured plaques had a low CT attenuation, compared with 18% of the stable lesions ($P<0.001$).[54] Similarly, other investigators have also reported lower

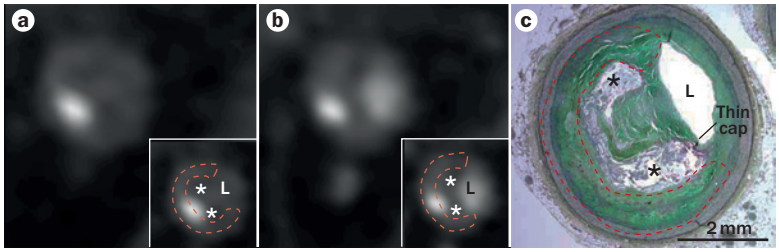

Figure 3 | Cross-sectional CT showing coronary plaque with napkin-ring sign and spotty calcification. The napkin-ring sign is a qualitative plaque feature, where the central area of low CT attenuation is apparently in contact with the lumen. The circumferential outer rim (red dashed line) of the noncalcified plaque has a higher CT attenuation. **a** | Non-contrast-enhanced cross-sectional CT. **b** | Contrast-enhanced cross sectional CT. **c** | Histopathology reveals a thin-cap fibroatheroma with spotty calcification. The necrotic core (stars) correlates with the low-attenuation plaque core on the CT images. The outer-rim attenuation (red dashed line) corresponds to the fibrous plaque tissue. Abbreviation: L, coronary lumen. Permission obtained from Elsevier © Maurovich-Horvat, P. *et al.* The napkin-ring sign: CT signature of high risk coronary plaques? *JACC Cardiovasc. Imaging* **3**, 440–445 (2010).[60]

mean CT densities of NCPs in patients with ACS versus SAP (40–86 HU versus 97–144 HU; $P<0.01$).[34,55,56]

Establishing a simple CT number cut-off value across an entire plaque that permits the reliable differentiation between lipid-rich and fibrous atherosclerotic lesions is difficult. However, quantification of CT number variability and identification of focal areas of low CT attenuation are methods that might aid a more-accurate differentiation of vulnerable plaques by CCTA. Moreover, culprit lesions in patients with ACS have significantly lower average CT numbers compared with patients who have SAP, suggesting that low CT attenuation is an established high-risk plaque feature.

Napkin-ring sign

Histopathological analysis of culprit and nonculprit TCFAs with similar stenosis revealed that only fibrous cap thickness (OR 0.35; $P<0.05$), and necrotic core size (OR 2.0; $P<0.02$) are independent predictors of plaque rupture.[14] A further analysis of the hierarchical importance of plaque features that are accessible by non-invasive imaging revealed that the size of necrotic core and the presence of macrophage infiltration are the two best discriminators between ruptured plaques or TCFAs and stable lesions.[14,15] Furthermore, a large necrotic core cross-sectional area (>3.5 mm^2) can differentiate a ruptured plaque or TCFA from a stable plaque.[15] In 80% of plaques vulnerable to rupture, the area of necrotic core is >1.0 mm^2.[19] These dimensions are over the detection threshold of CCTA and, therefore, enable noninvasive risk stratification of individual coronary plaques according the presence or absence of large necrotic core. A plaque cross-section with low CT attenuation in the central part of the lesion might be indicative of the presence of a large lipid-rich necrotic core.

A ring-like CT attenuation pattern of NCP was observed in ACS culprit plaques and in plaques associated with slow-flow and no re-flow phenomenon during percutaneous coronary intervention.[34,46,47,57–59] The term napkin-ring sign (NRS) is used to describe this specific plaque attenuation pattern.[60] The NRS is a qualitative plaque feature and can be defined in a noncalcified plaque cross-section by the presence of two features: a central area of low CT attenuation that is apparently in contact with the lumen; and a ring-like higher attenuation plaque tissue surrounding this central area (Figure 3).[60,61] Interestingly, NRS was present in both native (that is non-contrast-enhanced) and contrast-enhanced *ex vivo* CT images, suggesting that the feature is the result of differences in CT attenuation between the large necrotic core (a central low CT attenuation) and fibrous plaque tissue (ring-like higher attenuation).[60–62] However, *in vivo*, some additional factors (such as the vasa vasorum) might influence the development of NRS.[57] The area of necrotic core can be over twice the size in NRS plaques compared with non-NRS plaques (median 1.10 mm^2 versus 0.46 mm^2; $P=0.05$).[62] These values correlate with other histopathological observations that demonstrate the area of necrotic core in vulnerable plaques is >1.0 mm^2 in the majority (~80%) of cases.[19] In CT, the specificity of an NRS to identify an advanced coronary plaque and TCFA is excellent (98.9% and 94.1%, respectively).[61] In a detailed plaque attenuation pattern analysis, a pattern-based plaque classification scheme has been proposed that classifies noncalcified plaques into homogeneous and heterogeneous, and stratifies heterogeneous plaques into NRS and non-NRS lesions (Figure 4).[61,63] The diagnostic performance of pattern classification to identify advanced lesions was significantly better than conventional plaque classification made on the basis of calcified content (area under the receiver operating characteristics curve: 0.761 versus 0.678; $P<0.001$).[61] In clinical investigations the NRS had 96–100% specificity for the identification of TCFA or culprit ACS lesions.[34,46] The NRS was more frequent in TCFA compared with non-TCFA plaques defined by OCT in two different clinical studies (TCFA 44–65% versus non-TCFA 4–16%; $P<0.0001$).[46,47] NRS also independently predicted future ACS events (independently of positive remodelling and low attenuation) in a prospective study of 895 patients with a mean follow-up of 2.3 years (HR 5.6; $P<0.001$).[64]

The NRS seems to be a specific CT feature of plaques with a large necrotic core. However, the sensitivity of NRS is relatively low. A more-detailed analysis of different plaque attenuation patterns might provide means for the development of plaque classification scheme with improved diagnostic performance and identify vulnerable coronary plaques.

Positive remodelling

Rupture-prone plaques might not lead to significant luminal narrowing, owing to the effect of positive remodelling.[7] Positive remodelling describes the compensatory enlargement of the vessel wall that occurs at the site of the atherosclerotic lesion as the plaque size increases, resulting in the preservation of luminal area.[65] In histopathology studies, positive remodelling is associated with the abundance of macrophages and increased necrotic core.[66] CCTA can measure the outer vessel wall

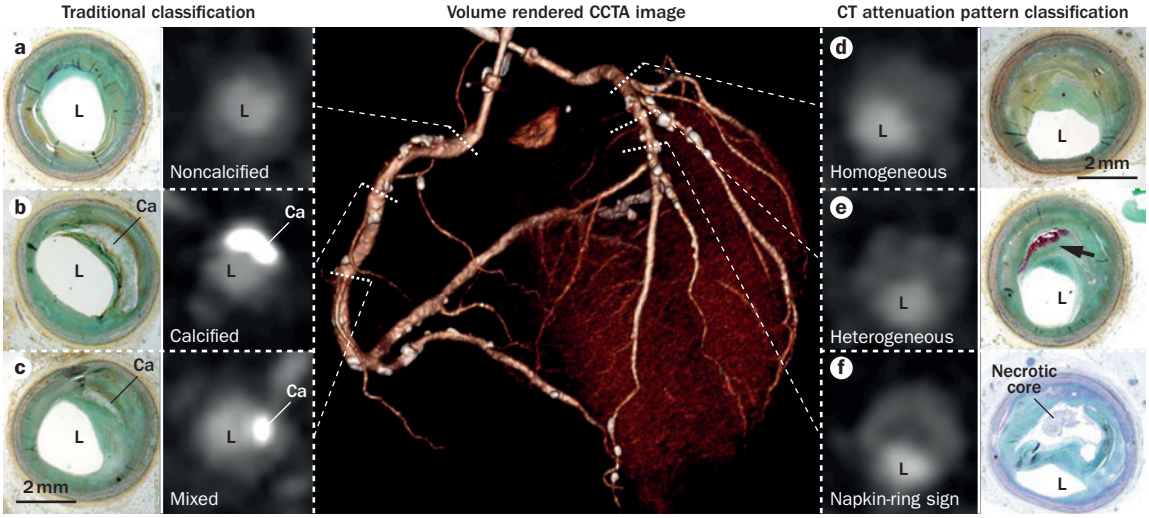

Figure 4 | Traditional and attenuation pattern-based plaque classification schemes in CCTA. The centre panel shows a volume-rendered CCTA image of a cadaver heart. The traditional plaque classification scheme differentiates between **a** | noncalcified, **b** | calcified, and **c** | partially calcified (mixed) plaques. CT attenuation pattern-based classification (right panel) differentiates between **d** | homogeneous, **e** | heterogeneous, and **f** | napkin-ring plaques. The corresponding histology slides show **a** | pathological intimal thickening, **b** | fibrous plaque with sheet calcification, **c** | pathological intimal thickening with spotty calcification, **d** | a fibrous plaque, **e** | early fibroatheroma with intraplaque haemorrhage (arrow), and **f** | a late fibroatheroma with large necrotic core. Abbreviations: Ca, calcium; L, lumen. Permission obtained from Elsevier © Maurovich-Horvat, P. *et al.* The napkin-ring sign indicates advanced atherosclerotic lesions in coronary CT angiography. *JACC Cardiovasc. Imag.* **5**, 1243–1252 (2012).[6]

and lumen dimension.[32,67–69] The remodelling index is calculated as the vessel cross-sectional area at the site of maximal stenosis divided by the average of proximal and distal reference segments' cross-sectional areas.[67,70] A remodelling index threshold of ≥1.1 was suggested for the definition of positive remodelling visualized by CCTA, whereas some authors use ≥1.05 or >1.0 as the cut-off point on the basis of IVUS studies.[68,70] Automated software now permits the easy quantification of the remodelling index.[30] The remodelling index assessed by CCTA correlates well with IVUS measurements; however, CCTA has a trend towards overestimation of remodelling index (95% CI of the mean difference 0.01–0.08; $P = 0.005$).[30,67,68] Consistent with histopathological data, lesions with positive remodelling on CCTA have a higher plaque burden, a larger amount of necrotic core and a higher prevalence of TCFA assessed by VH-IVUS when compared to lesions without positive remodelling.[71] Furthermore, in two correlative studies comparing CCTA with OCT, the CT-derived remodelling index was higher in TCFA compared with non-TCFA lesions classified by OCT (1.14 versus 1.02, $P < 0.0001$; and 1.14 versus 0.95, $P < 0.0001$).[46,47] A remodelling index threshold of 1.08, which had the best diagnostic performance to identify TCFA, has been suggested by some investigators.[47] In a study of 38 patients with ACS and 33 patients with SAP, positive remodelling was strongly associated with culprit plaques in ACS (87%), but not SAP (12%; $P < 0.0001$), and had the best diagnostic performance among other high-risk CT plaque features (low attenuation and spotty calcification) to identify the culprit lesions (sensitivity 87%; specificity 88%).[53] Several other cross-sectional CCTA studies have also found a higher remodelling index in patients with ACS compared with patients with SAP (1.14–1.6 versus 0.9–1.2; $P = 0.001–0.04$).[26,34,55,56] Positive plaque remodelling and/or low plaque attenuation was an independent predictor of ACS in a clinical study with 27 ± 10 months follow-up (HR 22.8; 95% CI 6.9–75.2; $P < 0.001$).[36] Among patients with one of these high-risk CT features, one in five will have an adverse coronary event within 1–3 years, a similar rate to those with a three-feature positive plaque determined by VH-IVUS in the PROSPECT trial.[24,36] The remodelling index can be reliably measured by CCTA. However, a more-conservative remodelling index threshold of 1.1 is preferred in the assessment of CCTA images.[68]

Spotty calcium in plaques

Calcification is an ever-present feature of advanced coronary atherosclerosis.[72] Coronary calcification assessed by CT is highly associated with plaque burden and related to poor clinical prognosis.[73,74] However, the effect of calcification on plaque instability is controversial.[75–77] Although most acute plaque ruptures in individuals with sudden cardiac death contain some calcification under histopathology, approximately two-thirds have only microcalcification, which is not detectable by CT.[78] In a serial IVUS study, plaques with heavy calcification are clinically quiescent, whereas spotty (small) calcification was associated with accelerated disease progression in patients with SAP.[79] Furthermore, the presence of spotty calcification was related to culprit plaques in patients with ACS in a study utilizing IVUS imaging.[80] In CCTA, spotty calcification is defined as a small, dense (>130 HU) plaque component surrounded by noncalcified plaque tissue. The typical cut-off to define

a small calcification in CCTA as spotty is <3 mm.[16,36,53] Spotty calcifications have been further differentiated into small (<1 mm), intermediate (1–3 mm), and large (>3 mm) calcifications.[81] Small spotty calcification has the strongest association with vulnerable plaque features defined by VH-IVUS.[81] Furthermore, in multiple cross-sectional studies in patients with ACS and SAP, spotty calcification is associated with ACS culprit lesions.[34,53–56] However, results vary widely, and highlight the current uncertainty in the relationship between spotty calcification and plaque rupture.[72] With further improvements in CT technology, detection of microcalcifications, which have been suggested to be a frequent feature in unstable angina, might be feasible.[82]

Functional plaque characteristics

Plaques develop at specific areas of coronary arteries where flow is disturbed, such as the outer walls of bifurcations, in side branches, and in the inner curve of arteries,[83–87] despite risk factors for plaque formation (including smoking, high cholesterol levels, hypertension, and insulin resistance) affecting the whole vascular bed.[83–87] Haemodynamic factors, such as endothelial shear stress (ESS), are pathologically important for the spatial localization and development of atherosclerotic plaques.[88] Low ESS promotes an atherogenic milieu and high-risk plaque formation, whereas high ESS at stenotic vulnerable plaque sites promotes plaque rupture by destabilization of the fibrous cap.[89–91]

In the early 1990s, *post-mortem* studies indicated that more than two-thirds of infarctions evolve from non-obstructive lesions (that is lesions occupying <70% of the lumen).[92] However, histopathological investigations have now challenged these studies, and a high portion of culprit lesions now seem to cause obstructive luminal narrowing (>75% area stenosis was seen in 70% of plaque ruptures), especially in late stages of plaque development before the disruption of the fibrous cap.[14,15,93] These observations correlate with evidence that patients with ischaemic lesions have a poor prognosis.[94,95] Indeed, increased plaque vulnerability might in part be a consequence of haemodynamic perturbations and altered shear stress owing to abnormal fractional flow reserve (FFR).[96] Invasive FFR is the gold standard method for the identification of lesions that result in ischaemia,[97] and the combination of ESS and FFR might, therefore, provide a novel functional dimension in plaque vulnerability assessment (Figure 1). Advances in computational fluid dynamics (CFD) have enabled the simulation of coronary flow and pressure-based metrics on the 3D geometry of the coronary artery tree.[98] When CFD is added to standardly acquired CCTA dataset, ESS-CT and FFR-CT coronary maps can be calculated.[99–101]

ESS-CT

ESS is the tangential force generated by the friction of flowing blood on the endothelial surface of the arterial wall.[102] In coronary artery segments with low and disturbed or turbulent flow—where ESS is low—the endothelial cell gene expression initiates a proatherogenic pattern.[103–104] Persistently low ESS reduces nitric oxide production, increases LDL uptake, promotes endothelial cell apoptosis, and induces local oxidative stress and inflammation, which induce an atherogenic endothelial phenotype and subsequently leads to the development of high-risk lesions.[86,88] By contrast, in straight arterial segments with undisturbed laminar flow—where ESS varies within a physiological range—endothelial cells express atheroprotective genes leading to plaque stability and quiescence.[87,88,102] However, high shear stress at the stenotic portion of the plaque might initiate pathophysiologic processes that promote plaque destabilization and rupture.[87,89] In serial IVUS studies of coronary arteries in diabetic pigs, the majority of vulnerable plaques developed in vessel segments characterized by persistently low ESS.[85,88,105] Furthermore, the magnitude of low ESS at baseline was significantly associated with the severity of high-risk plaque features at follow-up.[88] Another animal study has refined the concept that low ESS promotes coronary plaque growth and vulnerability by demonstrating that dyslipidaemia and low ESS have a synergistic effect leading to the development of vulnerable atheromas.[106]

The first natural-history VH-IVUS study in humans assessed the left anterior descending artery in 20 patients with nonobstructive CAD at enrolment and at 6 months follow-up.[90] Low ESS segments developed increased plaque area and necrotic core as well as constrictive remodelling, whereas high ESS segments developed greater necrotic core and regression of fibrous and fibrofatty tissue, and excessive positive remodelling, suggestive of transformation to a more-vulnerable phenotype.[90] These observations highlight the importance of low ESS in vulnerable plaque development and high ESS in the

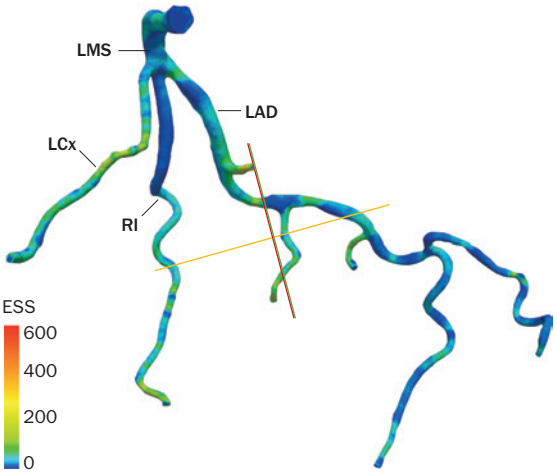

Figure 5 | Time averaged ESS map of a left coronary artery derived by computation fluid dynamics simulation. The ESS values are in dynes/cm^2. Dark-blue indicates low ESS values. Turquoise and green colours represent the normal physiological range of ESS. Yellow to red areas are regions of high ESS. Abbreviations: ESS, endothelial shear stress; LAD, left anterior descending artery; LCx, left circumflex coronary artery; LMS, left main stem; RI, ramus intermedius. Permission obtained from Alessandro Veneziani, Emory University, Atlanta, GA, USA.

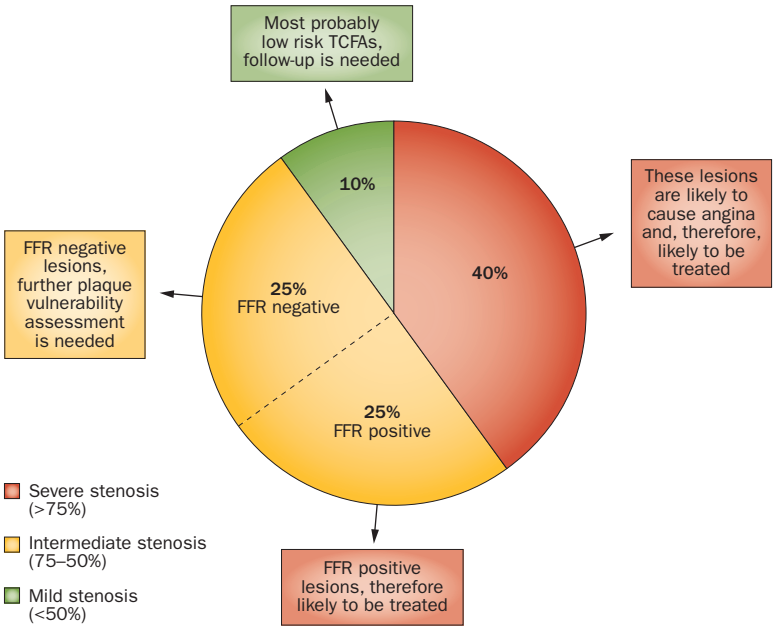

Figure 6 | In histopathological studies of patients who suffered sudden cardiac death, 40% of nonruptured TCFAs also caused >75% luminal narrowing. These TCFAs with significant luminal narrowing (>75%), are likely to cause angina, and therefore be treated. Lesions with an intermediate stenosis can be of danger, as they are large, but are not necessarily associated with symptoms. Vulnerable plaques with a stenosis range of 50–75% (~50% of TCFAs) are the real targets for noninvasive imaging. Abbreviations: FFR, fractional flow reserve; TCFA, thin cap fibroatheroma.

destabilization of these plaques. In the Prediction of Progression of Coronary Artery Disease and Clinical Outcome Using Vascular Profiling of Shear Stress and Wall Morphology (PREDICTION) trial,[107] a total of 506 patients underwent three-vessel IVUS examination and were assessed again at 1-year follow-up.[107] The results demonstrated that large plaque burden and low ESS can independently predict plaques that progressively enlarge and develop substantial lumen narrowing.[107]

3D coronary geometry visualization by CCTA enables CFD to be applied to ESS-CT calculations and subsequent coronary wall behaviour assessment (Figure 5).[101,108–110] These observations have been confirmed in a study using CCTA and IVUS for vascular profiling. CCTA was sufficiently accurate to determine ESS distribution in the main vessels and in the bifurcation regions.[111] The CFD simulations in CCTA can be used to remove all plaques in a virtual environment to replicate the healthy vascular wall before the development of atherosclerotic plaques. In an exploratory investigation, static and dynamic parameters of ESS-CT were calculated in a virtual healthy coronary lumen to determine the best haemodynamic predictor of future plaque location. The results of this virtual experiment suggested that low ESS is a prerequisite for plaque formation; however, its presence alone is insufficient to predict future plaque locations. Dynamic factors that describe the time-dependent directional changes in ESS might, therefore, have an incremental prognostic value regarding plaque progression and vulnerability.[112]

FFR-CT

Plaques that rupture cause substantial luminal narrowing at the time of the acute event. Histopathological investigations demonstrated that plaques that rupture but are nonstenotic are very rare.[14,15] The assessment of luminal narrowing at the site of a large lipid-rich plaque might, therefore, be an important addition to high-risk plaque features and could aid the identification of vulnerable plaques.

In a histopathological study of ruptured plaques and TCFAs, 70% produced significant narrowing (>75%) of the cross-sectional luminal area.[15] The remaining 30% of nonobstructive ruptured plaques were further subdivided into those with luminal narrowing of 50–75% and those with luminal narrowing <50% (25% and 5% of lesions respectively).[15] Importantly, the investigators assessed the nonruptured TCFAs, which are the potential targets for noninvasive imaging, and found 40% also caused luminal narrowing of >75%.[15] Because these lesions are likely to cause angina, they are probably more likely to be treated. However, lesions with an intermediate stenosis can be large, but not necessarily associated with symptoms of angina. Vulnerable plaques with a stenosis range of 50–75% (~50% of all TCFAs) are, therefore, the more-appropriate targets for noninvasive imaging (Figure 6). Notably, the relationship between intermediate stenosis (50–75% diameter stenosis) and the presence of ischaemia is extremely unreliable—half of the lesions lead to ischaemia and the remaining half do not, as determined by invasive FFR measurement.[113] In an intermediate lesion with abnormal FFR, the flow perturbations, altered ESS, and the physical strain changes placed on the plaque might be responsible for the development of a rupture-prone lesion.[96,114] Furthermore, patients with an obstructive coronary plaque might develop an ACS owing to thrombus formation induced by high EES.[115] In an investigation that included 70 patients with stable CAD, a strong association was observed between inflammatory cytokine activity and FFR; therefore, ischaemia might be involved in plaque progression and destabilization.[116] Moreover, in an explorative study, CCTA-visualized adverse features in obstructive plaques—that is, low attenuation plaque and positive remodelling—were strongly predictive of myocardial ischaemia.[117] TCFAs with intermediate stenosis and positive FFR should be treated; however, the noninvasive identification of these lesions is challenging. Conversely, <1% of patients with a plaque resulting in an intermediate stenosis without ischaemia (FFR ≥0.8) have a myocardial infarction within 5 years, which is similar to a matched control population without diagnosed CAD.[118]

FFR-CT will help in the identification of lesions with ischaemia and likely improve CT accuracy for the detection of high-risk lesions. Importantly, FFR-CT can be derived from CCTA, without the need for additional imaging, extra radiation, or any medication (Figure 7). Furthermore, FFR-CT provides a comprehensive three-vessel FFR from a single CCTA test, enabling FFR readings at any location of the coronary tree. Two prospective clinical trials have demonstrated that FFR-CT

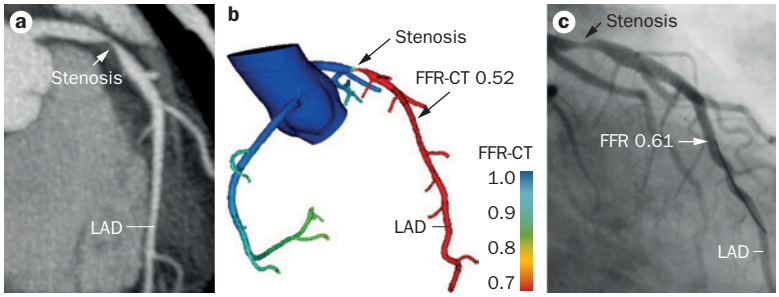

Figure 7 | FFR-CT compared with CCTA and coronary angiogram for the identification of significant stenoses. **a** | A multiplanar reformatted CCTA image indicating a noncalcified plaque with severe stenosis in the proximal LAD. **b** | A CFD derived FFR-CT map of the coronary artery tree, with an FFR-CT value of 0.52 distal to the stenosis, indicating lesion specific ischaemia. **c** | An invasive coronary angiogram that confirms the significant luminal narrowing with a measured FFR value of 0.61, which indicates ischaemia. Abbreviations: CCTA, coronary computed tomography angiography; CFD, computational fluid dynamics; FFR, fractional flow reserve; LAD, left anterior descending coronary artery. Permission obtained from Jonathon Leipsic, Providence Health Care, Vancouver, Canada.

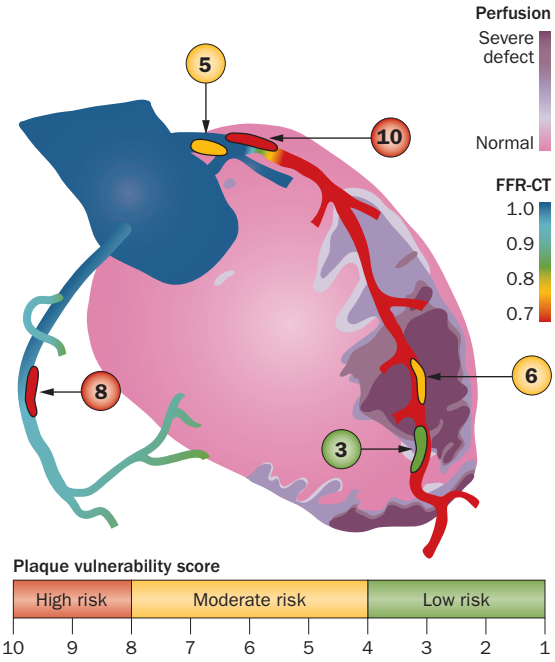

Figure 8 | An illustration of potential comprehensive plaque assessment with CCTA. The theoretical volume-rendered CT image consists of FFR-CT with myocardial perfusion imaging (pink indicates normally perfused myocardium, light purple represents moderate ischaemia, whereas purple indicates severe perfusion defect), which can differentiate between epicardial and small vessel disease. In this specific case epicardial disease can be confirmed as FFR-CT and the perfusion map show similar ischaemic regions. Each coronary plaque receives a vulnerability score based on morphological and functional data. In this vulnerability score, 1 represents a stable lesion (green) and 10 a high-risk, rupture prone plaque (red). The figure demonstrates that plaques with no haemodynamic significance might also contain high-risk characteristics and have an increased vulnerability score. Abbreviations: CCTA, coronary computed tomography angiography; FFR, fractional flow reserve.

compares favourably to the reference standard invasive FFR measurements.[119,120] In the Diagnosis of Ischemia-Causing Stenoses Obtained Via Noninvasive Fractional Flow Reserve (DISCOVER-FLOW) trial,[119] FFR-CT was compared with invasive FFR, and had a per-vessel accuracy of 84.3%, sensitivity of 87.9%, and specificity of 82.2%.[119] In addition, FFR-CT had better diagnostic performance than CCTA when identifying clinically significant coronary lesions; the area under the receiver-operator characteristics curve (AUC) were 0.90 for FFR-CT and 0.75 for CCTA ($P = 0.001$).[119] Investigators in the Determination of Fractional Flow Reserve by Anatomic Computed Tomographic Angiography (DeFACTO) trial,[120] a multicentre international study evaluating the diagnostic performance of FFR-CT, enrolled 252 patients. On a per-patient basis, FFR-CT was superior to CCTA in identifying ischaemic lesions (accuracy 73% versus 64%; sensitivity 90% versus 84%; specificity 54% versus 42%).[120] Compared with obstructive CAD diagnosed by CCTA alone (AUC 0.68; 95% CI 0.62–0.74), FFR-CT was associated with improved discrimination of coronary stenosis with ischaemia (AUC 0.81; 95% CI 0.75–0.86; $P < 0.001$).[120] Notably, in patients with intermediate stenosis, FFR-CT had more than a twofold increase in sensitivity compared with CCTA alone (82% versus 37%; no statistical data was reported), with no loss of specificity (66% versus 66%).[120] A novel application of CFD is the possibility of implanting a stent in a virtual setting to test different stenting strategies and predict functional outcomes by changes in FFR.[121] FFR-CT is an accurate new tool to assess lesion-specific ischaemia in a typically acquired CCTA exam and an improvement on the accuracy of CT alone.

Future directions for CCTA

Coupling individual plaque morphology with plaque specific functional data, including ESS and FFR, provide new opportunities for the noninvasive detection of plaques vulnerable to rupture. Combining morphological and functional metrics of coronary plaques (comprehensive plaque assessment) might lead to the development of a 'vulnerable plaque score' to indicate potential acute clinical events (Figure 8). Moreover, the high sensitivity and specificity of CCTA to identify atherosclerotic plaques can be combined with whole genome sequencing and epigenomics, whole transcriptome sequencing, unbiased proteomics, metabolomics, lipidomics, and lipoprotein proteomics to enable a stratified, step-wise approach ("omics' followed by CCTA if needed) to identify patients with subclinical CAD and vulnerable plaques, as in the Genetic Loci and the Burden of Atherosclerotic Lesions Study,[122] for example. Combining the complex information obtained from CT with bioinformatics analysis of genomic or proteomic data, as well as data derived from electronic medical records and drug information, might realize a personalized approach to cardiovascular disease prevention and care for each patient.[123–125]

Automated plaque assessment tools and computation fluid dynamics simulations will be necessary to provide multidimensional information on individual plaques. Importantly, the definition of vulnerable plaques by

CCTA has not yet been established. Large, longitudinal imaging trials to test the prognostic value of comprehensive plaque assessment and derive standardized CT metrics of vulnerable plaques are also warranted.

Using hybrid scanners and novel contrast agents to acquire metabolic information might also improve CT plaque assessment. For example, inflammatory immune cell infiltration into the fibrous cap is a strong marker of plaque rupture vulnerability.[7] In rabbits, the detection of inflammatory cells in atherosclerotic plaques by CCTA with iodinated nanoparticle contrast agent N1117 has been demonstrated.[126] Furthermore, spectral CT imaging of gold-labelled HDL nanoparticles targeted to activated macrophages showed promising results in a mouse model of atherosclerosis.[127] However, neither technique has been adapted for human patients. The high metabolic activity of macrophages and their metabolic dependence on exogenous glucose provide opportunity for combined positron emission tomography and CT imaging using a radiolabelled glucose analogue—fluorine-18-fluorodeoxyglucose (^{18}F-FDG)—to noninvasively detect vulnerable, inflamed plaques. In a clinical investigation `culprit lesion site of patients with recent ACS as compared to stented lesions in patients with SAP.[128] In a prospective clinical trial, ^{18}F-sodim fluoride (^{18}F-NaF) uptake co-localized to ruptured plaques in patients with ACS, and in patients with SAP ^{18}F-NaF identified plaques with high-risk features, as determined by IVUS.[82] The intriguing results showed that ^{18}F-NaF positron emission tomography-CT imaging can detect metabolically active plaques by identifying areas of ongoing calcification activity.[82]

Conclusion

CCTA has the ability to depict all main epicardial coronary branches and, therefore, enables both individual plaques and global coronary plaque burden to be evaluated. Modern CCTA assessment can identify multiple high-risk features—such as NRS, positive remodelling, low CT attenuation, and low ESS—that make a plaque vulnerable to rupture and, therefore, put individuals at increased risk of an acute cardiovascular event. Conversely, the limited spatial and contrast resolutions of CT scanners prevent the detection of some histological features of vulnerable plaques, such as fibrous cap thickness or plaque rupture. Nanoparticle contrast agents and hybrid imaging provide valuable information regarding the metabolic activity of atherosclerotic plaques, but initial results, although encouraging, need to be confirmed in large prospective trials. Patients with acute and stable chest pain syndromes—and perhaps even asymptomatic patients—might receive improved, targeted therapy and derive the health benefits from such interventions. However, CCTA uses ionizing radiation and its current use must, therefore, be limited to symptomatic patients with established clinical indication for this noninvasive test.

Generalized, large, prospective trials are needed to confirm the results of small, prospective or registry-based studies, because current data suggest that CCTA-based assessment of both individual and global coronary plaque features is highly predictive of future adverse events. Randomized trials testing whether interventions made on the basis of CCTA assessment can improve both health and economic outcomes should also be conducted. Further strategies targeting vulnerable plaques, or to treat patients more effectively, might also include medical therapy and/or plaque sealing with a biodegradable vascular scaffold.

Review criteria

English-language articles published between January 2000 and 2014 were identified by searching the PubMed database. The search criteria included were: "coronary ct angiography" or "non-invasive imaging", alone and in combination with "vulnerable plaque", "coronary plaque", "atherosclerotic plaque", "high-risk plaque", "computational fluid dynamics" and "functional assessment". Additional articles were identified from the reference lists of retrieved articles.

1. Mathers, C. D. & Loncar, D. Projections of global mortality and burden of disease from 2002 to 2030. *PLoS Med.* **3**, e442 (2006).
2. WHO. *Cardiovascular diseases (CVDs)* [online], http://www.who.int/mediacentre/factsheets/fs317/en/ (2013).
3. Go, A. S. *et al.* Heart disease and stroke statistics–2014 update: A report from the American Heart Association. *Circulation* **129**, e28–e292 (2014).
4. Heidenreich, P. A. *et al.* Forecasting the future of cardiovascular disease in the United States: a policy statement from the American Heart Association. *Circulation* **123**, 933–944 (2011).
5. Nabel, E. G. & Braunwald, E. A tale of coronary artery disease and myocardial infarction. *N. Engl. J. Med.* **366**, 54–63 (2012).
6. Libby, P. Mechanisms of acute coronary syndromes and their implications for therapy. *N. Engl. J. Med.* **368**, 2004–2013 (2013).
7. Narula, J. & Strauss, H. W. The popcorn plaques. *Nat. Med.* **13**, 532–534 (2007).
8. Braunwald, E. Epilogue: what do clinicians expect from imagers? *J. Am. Coll. Cardiol.* **47** (Suppl.), C101–C103 (2006).
9. Waxman, S., Ishibashi, F. & Muller, J. E. Detection and treatment of vulnerable plaques and vulnerable patients: novel approaches to prevention of coronary events. *Circulation* **114**, 2390–2411 (2006).
10. Burke, A. P. *et al.* Coronary risk factors and plaque morphology in men with coronary disease who died suddenly. *N. Engl. J. Med.* **336**, 1276–1282 (1997).
11. Falk, E., Nakano, M., Bentzon, J. F., Finn, A. V. & Virmani, R. Update on acute coronary syndromes: the pathologists' view. *Eur. Heart J.* **34**, 719–728 (2013).
12. Virmani, R., Kolodgie, F. D., Burke, A. P., Farb, A. & Schwartz, S. M. Lessons from sudden coronary death: a comprehensive morphological classification scheme for atherosclerotic lesions. *Arterioscler. Thromb. Vasc. Biol.* **20**, 1262–1275 (2000).
13. Narula, J. *et al.* Arithmetic of vulnerable plaques for noninvasive imaging. *Nat. Clin. Pract. Cardiovasc. Med.* **5** (Suppl. 2), S2–S10 (2008).
14. Finn, A. V., Nakano, M., Narula, J., Kolodgie, F. D. & Virmani, R. Concept of vulnerable/unstable plaque. *Arterioscler. Thromb. Vasc. Biol.* **30**, 1282–1292 (2010).
15. Narula, J. *et al.* Histopathologic characteristics of atherosclerotic coronary disease and implications of the findings for the invasive and noninvasive detection of vulnerable plaques. *J. Am. Coll. Cardiol.* **61**, 1041–1051 (2013).
16. Ferencik, M. *et al.* A computed tomography-based coronary lesion score to predict acute coronary syndrome among patients with acute chest pain and significant coronary stenosis on coronary computed tomographic angiogram. *Am. J. Cardiol.* **110**, 183–189 (2012).
17. Achenbach, S. *et al.* CV Imaging: What was new in 2012? *JACC Cardiovasc. Imaging* **6**, 714–734 (2013).
18. Achenbach, S. & Raggi, P. Imaging of coronary atherosclerosis by computed tomography. *Eur. Heart J.* **31**, 1442–1448 (2010).

19. Virmani, R., Burke, A. P., Farb, A. & Kolodgie, F. D. Pathology of the vulnerable plaque. *J. Am. Coll. Cardiol.* **47** (Suppl.), C13–C18 (2006).
20. Achenbach, S. Can CT detect the vulnerable coronary plaque? *Int. J. Cardiovasc. Imaging* **24**, 311–312 (2008).
21. Kolodgie, F. D. *et al.* The thin-cap fibroatheroma: a type of vulnerable plaque: the major precursor lesion to acute coronary syndromes. *Curr. Opin. Cardiol.* **16**, 285–292 (2001).
22. van der Giessen, A. G. *et al.* Reproducibility, accuracy, and predictors of accuracy for the detection of coronary atherosclerotic plaque composition by computed tomography: an *ex vivo* comparison to intravascular ultrasound. *Invest. Radiol.* **45**, 693–701 (2010).
23. Hoffmann, U., Ferencik, M., Cury, R. C. & Pena, A. J. Coronary CT angiography. *J. Nucl. Med.* **47**, 797–806 (2006).
24. Stone, G. W. *et al.* A prospective natural-history study of coronary atherosclerosis. *N. Engl. J. Med.* **364**, 226–235 (2011).
25. Blackmon, K. N. *et al.* Reproducibility of automated noncalcified coronary artery plaque burden assessment at coronary CT angiography. *J. Thorac. Imaging* **24**, 96–102 (2009).
26. Hoffmann, U. *et al.* Noninvasive assessment of plaque morphology and composition in culprit and stable lesions in acute coronary syndrome and stable lesions in stable angina by multidetector computed tomography. *J. Am. Coll. Cardiol.* **47**, 1655–1662 (2006).
27. Klass, O. *et al.* Coronary plaque imaging with 256-slice multidetector computed tomography: interobserver variability of volumetric lesion parameters with semiautomatic plaque analysis software. *Int. J. Cardiovasc. Imaging* **26**, 711–720 (2010).
28. Brodoefel, H. *et al.* Coronary plaque quantification by voxel analysis: dual-source MDCT angiography versus intravascular sonography. *AJR Am. J. Roentgenol.* **192**, W84–W89 (2009).
29. Schepis, T. *et al.* Quantification of non-calcified coronary atherosclerotic plaques with dual-source computed tomography: comparison with intravascular ultrasound. *Heart* **96**, 610–615 (2010).
30. Boogers, M. J. *et al.* Automated quantification of coronary plaque with computed tomography: comparison with intravascular ultrasound using a dedicated registration algorithm for fusion-based quantification. *Eur. Heart J.* **33**, 1007–1016 (2012).
31. Voros, S. *et al.* Prospective validation of standardized, 3-dimensional, quantitative coronary computed tomographic plaque measurements using radiofrequency backscatter intravascular ultrasound as reference standard in intermediate coronary arterial lesions: results from the ATLANTA (assessment of tissue characteristics, lesion morphology, and hemodynamics by angiography with fractional flow reserve, intravascular ultrasound and virtual histology, and noninvasive computed tomography in atherosclerotic plaques) I study. *JACC Cardiovasc. Interv.* **4**, 198–208 (2011).
32. Voros, S. *et al.* Coronary atherosclerosis imaging by coronary CT angiography: current status, correlation with intravascular interrogation and meta-analysis. *JACC Cardiovasc. Imaging* **4**, 537–548 (2011).
33. Oberoi, S. *et al.* Reproducibility of noncalcified coronary artery plaque burden quantification from coronary CT angiography across different image analysis platforms. *AJR Am. J. Roentgenol.* **202**, W43–W49 (2014).
34. Pflederer, T. *et al.* Characterization of culprit lesions in acute coronary syndromes using coronary dual-source CT angiography. *Atherosclerosis* **211**, 437–444 (2010).
35. Madder, R. D., Chinnaiyan, K. M., Marandici, A. M. & Goldstein, J. A. Features of disrupted plaques by coronary computed tomographic angiography: correlates with invasively proven complex lesions. *Circ. Cardiovasc. Imaging* **4**, 105–113 (2011).
36. Motoyama, S. *et al.* Computed tomographic angiography characteristics of atherosclerotic plaques subsequently resulting in acute coronary syndrome. *J. Am. Coll. Cardiol.* **54**, 49–57 (2009).
37. Versteylen, M. O. *et al.* Additive value of semiautomated quantification of coronary artery disease using cardiac computed tomographic angiography to predict future acute coronary syndrome. *J. Am. Coll. Cardiol.* **61**, 2296–2305 (2013).
38. Kristensen, T. S. *et al.* Prognostic implications of nonobstructive coronary plaques in patients with non-ST-segment elevation myocardial infarction: a multidetector computed tomography study. *J. Am. Coll. Cardiol.* **58**, 502–509 (2011).
39. Papadopoulou, S. L. *et al.* Natural history of coronary atherosclerosis by multislice computed tomography. *JACC Cardiovasc. Imaging* **5** (Suppl.), S28–S37 (2012).
40. Schlett, C. L. *et al.* How to assess non-calcified plaque in CT angiography: delineation methods affect diagnostic accuracy of low-attenuation plaque by CT for lipid-core plaque in histology. *Eur. Heart J. Cardiovasc. Imaging* **14**, 1099–1105 (2013).
41. Becker, C. R., Knez, A., Ohnesorge, B., Schoepf, U. J. & Reiser, M. F. Imaging of noncalcified coronary plaques using helical CT with retrospective ECG gating. *AJR Am. J. Roentgenol.* **175**, 423–424 (2000).
42. Achenbach, S. *et al.* Detection of calcified and noncalcified coronary atherosclerotic plaque by contrast-enhanced, submillimeter multidetector spiral computed tomography: a segment-based comparison with intravascular ultrasound. *Circulation* **109**, 14–17 (2004).
43. Pohle, K. *et al.* Characterization of non-calcified coronary atherosclerotic plaque by multi-detector row CT: comparison to IVUS. *Atherosclerosis* **190**, 174–180 (2007).
44. Marwan, M. *et al. In vivo* CT detection of lipid-rich coronary artery atherosclerotic plaques using quantitative histogram analysis: a head to head comparison with IVUS. *Atherosclerosis* **215**, 110–115 (2011).
45. Schlett, C. L. *et al.* Histogram analysis of lipid-core plaques in coronary computed tomographic angiography: *ex vivo* validation against histology. *Invest. Radiol.* **48**, 646–653 (2013).
46. Kashiwagi, M. *et al.* Feasibility of noninvasive assessment of thin-cap fibroatheroma by multidetector computed tomography. *JACC Cardiovasc. Imaging* **2**, 1412–1419 (2009).
47. Ito, T. *et al.* Comparison of *in vivo* assessment of vulnerable plaque by 64-slice multislice computed tomography versus optical coherence tomography. *Am. J. Cardiol.* **107**, 1270–1277 (2011).
48. Achenbach, S. *et al.* Influence of slice thickness and reconstruction kernel on the computed tomographic attenuation of coronary atherosclerotic plaque. *J. Cardiovasc. Comput. Tomogr.* **4**, 110–115 (2010).
49. Cademartiri, F. *et al.* Influence of intracoronary attenuation on coronary plaque measurements using multislice computed tomography: observations in an *ex vivo* model of coronary computed tomography angiography. *Eur. Radiol.* **15**, 1426–1431 (2005).
50. Ferencik, M. *et al.* Arterial wall imaging: evaluation with 16-section multidetector CT in blood vessel phantoms and *ex vivo* coronary arteries. *Radiology* **240**, 708–716 (2006).
51. Suzuki, S. *et al.* Accuracy of attenuation measurement of vascular wall *in vitro* on computed tomography angiography: effect of wall thickness, density of contrast medium, and measurement point. *Invest. Radiol.* **41**, 510–515 (2006).
52. Dey, D. *et al.* Automated three-dimensional quantification of noncalcified coronary plaque from coronary CT angiography: comparison with intravascular US. *Radiology* **257**, 516–522 (2010).
53. Motoyama, S. *et al.* Multislice computed tomographic characteristics of coronary lesions in acute coronary syndromes. *J. Am. Coll. Cardiol.* **50**, 319–326 (2007).
54. Ozaki, Y. *et al.* Coronary CT angiographic characteristics of culprit lesions in acute coronary syndromes not related to plaque rupture as defined by optical coherence tomography and angioscopy. *Eur. Heart J.* **32**, 2814–2823 (2011).
55. Kim, S. Y. *et al.* The culprit lesion score on multi-detector computed tomography can detect vulnerable coronary artery plaque. *Int. J. Cardiovasc. Imaging* **26** (Suppl. 2), 245–252 (2010).
56. Kitagawa, T. *et al.* Characterization of noncalcified coronary plaques and identification of culprit lesions in patients with acute coronary syndrome by 64-slice computed tomography. *JACC Cardiovasc. Imaging* **2**, 153–160 (2009).
57. Nakazawa, G. *et al.* Efficacy of culprit plaque assessment by 64-slice multidetector computed tomography to predict transient no-reflow phenomenon during percutaneous coronary intervention. *Am. Heart J.* **155**, 1150–1157 (2008).
58. Kodama, T., Kondo, T., Oida, A., Fujimoto, S. & Narula, J. Computed tomographic angiography-verified plaque characteristics and slow-flow phenomenon during percutaneous coronary intervention. *JACC Cardiovasc. Interv.* **5**, 636–643 (2012).
59. Tanaka, A. *et al.* Non-invasive assessment of plaque rupture by 64-slice multidetector computed tomography–comparison with intravascular ultrasound. *Circ. J.* **72**, 1276–1281 (2008).
60. Maurovich-Horvat, P. *et al.* The napkin-ring sign: CT signature of high risk coronary plaques? *JACC Cardiovasc. Imaging* **3**, 440–444 (2010).
61. Maurovich-Horvat, P. *et al.* The napkin-ring sign indicates advanced atherosclerotic lesions in coronary CT angiography. *JACC Cardiovasc. Imaging* **5**, 1243–1252 (2012).
62. Seifarth, H. *et al.* Histopathological correlates of the napkin-ring sign plaque in coronary CT angiography. *Atherosclerosis* **224**, 90–96 (2012).
63. Yamamoto, H., Kitagawa, T. & Kihara, Y. Dose napkin-ring sign suggest possibility to identify rupture-prone plaque in coronary computed tomography angiography? *J. Cardiol.* **62**, 328–329 (2013).
64. Otsuka, K. *et al.* Napkin-ring sign on coronary CT angiography for the prediction of acute coronary syndrome. *JACC Cardiovasc. Imaging* **6**, 448–457 (2013).
65. Glagov, S., Weisenberg, E., Zarins, C. K., Stankunavicius, R. & Kolettis, G. J. Compensatory enlargement of human atherosclerotic coronary arteries. *N. Engl. J. Med.* **316**, 1371–1375 (1987).

66. Varnava, A. M., Mills, P. G. & Davies, M. J. Relationship between coronary artery remodeling and plaque vulnerability. *Circulation* **105**, 939–943 (2002).
67. Achenbach, S. *et al.* Assessment of coronary remodeling in stenotic and nonstenotic coronary atherosclerotic lesions by multidetector spiral computed tomography. *J. Am. Coll. Cardiol.* **43**, 842–847 (2004).
68. Gauss, S. *et al.* Assessment of coronary artery remodelling by dual-source CT: a head-to-head comparison with intravascular ultrasound. *Heart* **97**, 991–997 (2011).
69. Moselewski, F. *et al.* Comparison of measurement of cross-sectional coronary atherosclerotic plaque and vessel areas by 16-slice multidetector computed tomography versus intravascular ultrasound. *Am. J. Cardiol.* **94**, 1294–1297 (2004).
70. Mintz, G. S. *et al.* American College of Cardiology clinical expert consensus document on standards for acquisition, measurement and reporting of intravascular ultrasound studies (IVUS). A report of the American College of Cardiology Task Force on clinical expert consensus documents. *J. Am. Coll. Cardiol.* **37**, 1478–1492 (2001).
71. Kröner, E. S. *et al.* Positive remodeling on coronary computed tomography as a marker for plaque vulnerability on virtual histology intravascular ultrasound. *Am. J. Cardiol.* **107**, 1725–1729 (2011).
72. Otsuka, F., Finn, A. V. & Virmani, R. Do vulnerable and ruptured plaques hide in heavily calcified arteries? *Atherosclerosis* **229**, 34–37 (2013).
73. Greenland, P., LaBree, L., Azen, S. P., Doherty, T. M. & Detrano, R. C. Coronary artery calcium score combined with Framingham score for risk prediction in asymptomatic individuals. *JAMA* **291**, 210–215 (2004).
74. Taylor, A. J. *et al.* Coronary calcium independently predicts incident premature coronary heart disease over measured cardiovascular risk factors: mean three-year outcomes in the Prospective Army Coronary Calcium (PACC) project. *J. Am. Coll. Cardiol.* **46**, 807–814 (2005).
75. Huang, H. *et al.* The impact of calcification on the biomechanical stability of atherosclerotic plaques. *Circulation* **103**, 1051–1056 (2001).
76. Maldonado, N. *et al.* A mechanistic analysis of the role of microcalcifications in atherosclerotic plaque stability: potential implications for plaque rupture. *Am. J. Physiol. Heart Circ. Physiol.* **303**, H619–H628 (2012).
77. Mauriello, A. *et al.* Coronary calcification identifies the vulnerable patient rather than the vulnerable plaque. *Atherosclerosis* **229**, 124–129 (2013).
78. Burke, A. P. *et al.* Pathophysiology of calcium deposition in coronary arteries. *Herz* **26**, 239–244 (2001).
79. Kataoka, Y. *et al.* Spotty calcification as a marker of accelerated progression of coronary atherosclerosis: insights from serial intravascular ultrasound. *J. Am. Coll. Cardiol.* **59**, 1592–1597 (2012).
80. Ehara, S. *et al.* Spotty calcification typifies the culprit plaque in patients with acute myocardial infarction: an intravascular ultrasound study. *Circulation* **110**, 3424–3429 (2004).
81. van Velzen, J. E. *et al.* Comprehensive assessment of spotty calcifications on computed tomography angiography: comparison to plaque characteristics on intravascular ultrasound with radiofrequency backscatter analysis. *J. Nucl. Cardiol.* **18**, 893–903 (2011).
82. Joshi, N. V. *et al.* 18F-fluoride positron emission tomography for identification of ruptured and high-risk coronary atherosclerotic plaques: a prospective clinical trial. *Lancet* **383**, 705–713 (2014).
83. Caro, C. G., Fitz-Gerald, J. M. & Schroter, R. C. Arterial wall shear and distribution of early atheroma in man. *Nature* **223**, 1159–1160 (1969).
84. Friedman, M. H., Bargeron, C. B., Deters, O. J., Hutchins, G. M. & Mark, F. F. Correlation between wall shear and intimal thickness at a coronary artery branch. *Atherosclerosis* **68**, 27–33 (1987).
85. Koskinas, K. C. *et al.* Natural history of experimental coronary atherosclerosis and vascular remodeling in relation to endothelial shear stress: a serial, *in vivo* intravascular ultrasound study. *Circulation* **121**, 2092–2101 (2010).
86. Malek, A. M., Alper, S. L. & Izumo, S. Hemodynamic shear stress and its role in atherosclerosis. *JAMA* **282**, 2035–2042 (1999).
87. Wentzel, J. J. *et al.* Endothelial shear stress in the evolution of coronary atherosclerotic plaque and vascular remodelling: current understanding and remaining questions. *Cardiovasc. Res.* **96**, 234–243 (2012).
88. Chatzizisis, Y. S. *et al.* Role of endothelial shear stress in the natural history of coronary atherosclerosis and vascular remodeling: molecular, cellular, and vascular behavior. *J. Am. Coll. Cardiol.* **49**, 2379–2393 (2007).
89. Slager, C. J. *et al.* The role of shear stress in the destabilization of vulnerable plaques and related therapeutic implications. *Nat. Clin. Pract. Cardiovasc. Med.* **2**, 456–464 (2005).
90. Samady, H. *et al.* Coronary artery wall shear stress is associated with progression and transformation of atherosclerotic plaque and arterial remodeling in patients with coronary artery disease. *Circulation* **124**, 779–788 (2011).
91. Fukumoto, Y. *et al.* Localized elevation of shear stress is related to coronary plaque rupture: a 3-dimensional intravascular ultrasound study with in-vivo color mapping of shear stress distribution. *J. Am. Coll. Cardiol.* **51**, 645–650 (2008).
92. Falk, E., Shah, P. K. & Fuster, V. Coronary plaque disruption. *Circulation* **92**, 657–671 (1995).
93. Puri, R., Nicholls, S. J., Ellis, S. G., Tuzcu, E. M. & Kapadia, S. R. High-risk coronary atheroma: the interplay between ischemia, plaque burden, and disease progression. *J. Am. Coll. Cardiol.* **63**, 1134–1140 (2014).
94. Hachamovitch, R. *et al.* Incremental prognostic value of myocardial perfusion single photon emission computed tomography for the prediction of cardiac death: differential stratification for risk of cardiac death and myocardial infarction. *Circulation* **97**, 535–543 (1998).
95. Shaw, L. J. *et al.* Optimal medical therapy with or without percutaneous coronary intervention to reduce ischemic burden: results from the Clinical Outcomes Utilizing Revascularization and Aggressive Drug Evaluation (COURAGE) trial nuclear substudy. *Circulation* **117**, 1283–1291 (2008).
96. Fearon, W. F. Is a myocardial infarction more likely to result from a mild coronary lesion or an ischemia-producing one? *Circ. Cardiovasc. Interv.* **4**, 539–541 (2011).
97. Fihn, S. D. *et al.* 2012 ACCF/AHA/ACP/AATS/PCNA/SCAI/STS Guideline for the diagnosis and management of patients with stable ischemic heart disease: a report of the American College of Cardiology Foundation/American Heart Association Task Force on Practice Guidelines, and the American College of Physicians, American Association for Thoracic Surgery, Preventive Cardiovascular Nurses Association, Society for Cardiovascular Angiography and Interventions, and Society of Thoracic Surgeons. *J. Am. Coll. Cardiol.* **60**, e44–e164 (2012).
98. Kim, H. J. *et al.* Patient-specific modeling of blood flow and pressure in human coronary arteries. *Ann. Biomed. Eng.* **38**, 3195–3209 (2010).
99. Taylor, C. A., Fonte, T. A. & Min, J. K. Computational fluid dynamics applied to cardiac computed tomography for noninvasive quantification of fractional flow reserve: scientific basis. *J. Am. Coll. Cardiol.* **61**, 2233–2241 (2013).
100. Nieman, K. & de Feijter, P. J. Aerodynamics in cardiac CT. *Circ. Cardiovasc. Imaging* **6**, 853–854 (2013).
101. Ramkumar, P. G., Mitsouras, D., Feldman, C. L., Stone, P. H. & Rybicki, F. J. New advances in cardiac computed tomography. *Curr. Opin. Cardiol.* **24**, 596–603 (2009).
102. Slager, C. J. *et al.* The role of shear stress in the generation of rupture-prone vulnerable plaques. *Nat. Clin. Pract Cardiovasc. Med.* **2**, 401–407 (2005).
103. Gimbrone, M. A. Jr, Topper, J. N., Nagel, T., Anderson, K. R. & Garcia-Cardena, G. Endothelial dysfunction, hemodynamic forces, and atherogenesis. *Ann. N Y Acad. Sci.* **902**, 230–239 (2000).
104. Brooks, A. R., Lelkes, P. I. & Rubanyi, G. M. Gene expression profiling of human aortic endothelial cells exposed to disturbed flow and steady laminar flow. *Physiol. Genomics* **9**, 27–41 (2002).
105. Chatzizisis, Y. S. *et al.* Augmented expression and activity of extracellular matrix-degrading enzymes in regions of low endothelial shear stress colocalize with coronary atheromata with thin fibrous caps in pigs. *Circulation* **123**, 621–630 (2011).
106. Koskinas, K. C. *et al.* Synergistic effect of local endothelial shear stress and systemic hypercholesterolemia on coronary atherosclerotic plaque progression and composition in pigs. *Int. J. Cardiol.* **169**, 394–401 (2013).
107. Stone, P. H. *et al.* Prediction of progression of coronary artery disease and clinical outcomes using vascular profiling of endothelial shear stress and arterial plaque characteristics: the PREDICTION Study. *Circulation* **126**, 172–181 (2012).
108. Frauenfelder, T. *et al.* In-vivo flow simulation in coronary arteries based on computed tomography datasets: feasibility and initial results. *Eur. Radiol.* **17**, 1291–1300 (2007).
109. Jin, S. *et al.* Flow patterns and wall shear stress distributions at atherosclerotic-prone sites in a human left coronary artery–an exploration using combined methods of CT and computational fluid dynamics. *Conf. Proc. IEEE Eng. Med. Biol. Soc.* **5**, 3789–3791 (2004).
110. Borkin, M. A. *et al.* Evaluation of artery visualizations for heart disease diagnosis. *IEEE Trans. Vis. Comput. Graph.* **17**, 2479–2488 (2011).
111. Gijsen, F. J. *et al.* 3D reconstruction techniques of human coronary bifurcations for shear stress computations. *J. Biomech.* **47**, 39–43 (2014).
112. Rikhtegar, F. *et al.* Choosing the optimal wall shear parameter for the prediction of plaque location-A patient-specific computational study in human left coronary arteries. *Atherosclerosis* **221**, 432–437 (2012).

113. Bech, G. J. *et al.* Fractional flow reserve to determine the appropriateness of angioplasty in moderate coronary stenosis: a randomized trial. *Circulation* **103**, 2928–2934 (2001).
114. Gijsen, F. J. *et al.* Strain distribution over plaques in human coronary arteries relates to shear stress. *Am. J. Physiol. Heart Circ. Physiol.* **295**, H1608–H1614 (2008).
115. Yong, A. S. *et al.* Intracoronary shear-related up-regulation of platelet P-selectin and platelet-monocyte aggregation despite the use of aspirin and clopidogrel. *Blood* **117**, 11–20 (2011).
116. Versteeg, D. *et al.* Monocyte toll-like receptor 2 and 4 responses and expression following percutaneous coronary intervention: association with lesion stenosis and fractional flow reserve. *Heart* **94**, 770–776 (2008).
117. Shmilovich, H. *et al.* Vulnerable plaque features on coronary CT angiography as markers of inducible regional myocardial hypoperfusion from severe coronary artery stenoses. *Atherosclerosis* **219**, 588–595 (2011).
118. Muller, O. *et al.* Long-term follow-up after fractional flow reserve-guided treatment strategy in patients with an isolated proximal left anterior descending coronary artery stenosis. *JACC Cardiovasc. Interv.* **4**, 1175–1182 (2011).
119. Koo, B. K. *et al.* Diagnosis of ischemia-causing coronary stenoses by noninvasive fractional flow reserve computed from coronary computed tomographic angiograms. Results from the prospective multicenter DISCOVER-FLOW (Diagnosis of Ischemia-Causing Stenoses Obtained Via Noninvasive Fractional Flow Reserve) study. *J. Am. Coll. Cardiol.* **58**, 1989–1997 (2011).
120. Min, J. K. *et al.* Diagnostic accuracy of fractional flow reserve from anatomic CT angiography. *JAMA* **308**, 1237–1245 (2012).
121. Kim, K. H. *et al.* A novel noninvasive technology for treatment planning using virtual coronary stenting and computed tomography-derived computed fractional flow reserve. *JACC Cardiovasc. Interv.* **7**, 72–78 (2014).
122. US National Library of Medicine. *Clinicaltrials.gov* [online], http://www.clinicaltrials.gov/ct2/show/NCT01738828?term=GLOBAL&rank=1 (2014).
123. Narula, J. Are we up to speed?: from big data to rich insights in CV imaging for a hyperconnected world. *JACC Cardiovasc. Imaging* **6**, 1222–1224 (2013).
124. Joshi, P. H. *et al.* A peripheral blood gene expression score is associated with plaque volume and phenotype by intravascular ultrasound with radiofrequency backscatter analysis: results from the ATLANTA study. *Cardiovasc. Diagn. Ther.* **3**, 5–14 (2013).
125. Voros, S. *et al.* Apoprotein B, small-dense LDL and impaired HDL remodeling is associated with larger plaque burden and more noncalcified plaque as assessed by coronary CT angiography and intravascular ultrasound with radiofrequency backscatter: results from the ATLANTA I study. *J. Am. Heart Assoc.* **2**, e000344 (2013).
126. Hyafil, F. *et al.* Noninvasive detection of macrophages using a nanoparticulate contrast agent for computed tomography. *Nat. Med.* **13**, 636–641 (2007).
127. Cormode, D. P. *et al.* Atherosclerotic plaque composition: analysis with multicolor CT and targeted gold nanoparticles. *Radiology* **256**, 774–782 (2010).
128. Rogers, I. S. *et al.* Feasibility of FDG imaging of the coronary arteries: comparison between acute coronary syndrome and stable angina. *JACC Cardiovasc. Imaging* **3**, 388–397 (2010).

Acknowledgements

P.M-H. acknowledges support from the European Union, State of Hungary, and European Social Fund in the framework of TÁMOP 4.2.4. A/1-11-1-2012-0001 'National Excellence Program'. M.F. acknowledges support from the American Heart Association (grant number: 13FTF16450001).

Author contributions

The authors contributed equally to researching data for the article, discussion of content, writing, reviewing, and editing of the manuscript before submission.